

RSC Advances



This is an *Accepted Manuscript*, which has been through the Royal Society of Chemistry peer review process and has been accepted for publication.

Accepted Manuscripts are published online shortly after acceptance, before technical editing, formatting and proof reading. Using this free service, authors can make their results available to the community, in citable form, before we publish the edited article. This *Accepted Manuscript* will be replaced by the edited, formatted and paginated article as soon as this is available.

You can find more information about *Accepted Manuscripts* in the [Information for Authors](#).

Please note that technical editing may introduce minor changes to the text and/or graphics, which may alter content. The journal's standard [Terms & Conditions](#) and the [Ethical guidelines](#) still apply. In no event shall the Royal Society of Chemistry be held responsible for any errors or omissions in this *Accepted Manuscript* or any consequences arising from the use of any information it contains.



Journal Name

ARTICLE

The role of Br in the selective synthesis of thin-walled carbon-nanotubes with micrometre-length Fe₃C-filling, Fe₃C tip-filled carbon-nanotubes or empty carbon-nanotubes by pyrolysis of ferrocene and (6-Bromohexyl)ferrocene mixtures

Received 00th January 20xx,
Accepted 00th January 20xx

DOI: 10.1039/x0xx00000x

www.rsc.org/

J. Guo,^{+a} Y. He,^b Lan Mu^a, S.Wang,^b Zhichao Weng^a, G.Xiang^{a**} and Filippo S.Boi,^{+a*}

We report an advanced chemical vapour deposition method which allows the synthesis-selection of thin walled carbon nanotubes filled with micrometre-length Fe₃C single crystals, Fe₃C tip-filled nanotubes or of empty thin walled carbon nanotubes by controlled addition of a not previously used precursor (6-Bromohexyl)ferrocene to ferrocene.

Since their discovery, carbon nanotubes (CNTs) have attracted a great attention owing to their extremely high stiffness¹, very large electrical conductivity properties^{1,2} and very high chemical stability³⁻⁶. These exceptional properties make these nanostructures suitable candidates for numerous applications involving the creation of extremely stiff building blocks^{1,2}, supercapacitors, electrodes, energy storage systems,³⁻⁵ films with extremely high conductivity (buckypapers)³⁻⁵ and capsules for magnetic crystals⁶, allowing the complete protection of the encapsulated material from the external environment. Particularly in the last decade, CNTs have indeed been filled with numerous magnetic materials, in particular metals like α -Fe and alloys like Fe₃C, FeNi, FeCo, FeNiCo through chemical vapour deposition (CVD) approaches involving the sublimation and pyrolysis of metallocene molecules (typically ferrocene, cobaltocene or nickelocene)⁶⁻¹⁶. However previous studies have shown that CVD of the only metallocenes (in laminar Ar flow conditions) can not allow the control of the CNTs filling-rate owing to the fixed carbon to metal ratio (10:1). Several solutions to this problem have then recently been proposed: CVD of ferrocene in locally perturbed vapours flow conditions¹⁷, pyrolysis of ferrocene

and/or nickelocene in viscous boundary layers created between a rough surface and a laminar vapour flow¹⁸⁻¹⁹, and CVD of ferrocene and trichlorobenzene (or similar Cl-containing benzene structures) mixtures²⁰⁻²⁵. In this context the latter approach has attracted a great attention owing to the key role played by Cl in the CVD reaction. Indeed it has been suggested that Cl can slow down the saturation-rate of the Fe-based catalyst by removing carbon feedstock through the formation of carbon chlorinated clusters CCl₄ which will then adjust the carbon to metal ratio in the reaction, favouring therefore the growth of CNTs with high filling rates. Furthermore it has been suggested that the combination of H and Cl atoms can lead to the formation of HCl which at high temperatures (in the form of Cl-radicals) will etch the walls of the CNTs, allowing the growth of thin walled CNTs structures²³⁻²⁴. However, despite the recent reports based on this approach, to the best of our knowledge no work has been performed on the specific case of Br and on its role in the control of the filling rate of the CNTs. In this paper, we report an advanced CVD approach which involves the sublimation and pyrolysis of mixtures of ferrocene with a not previously studied precursor: (6-Bromohexyl)ferrocene. Thanks to its metallocene-like structure and its low sublimation temperature (200-300 °C) this compound can be used to carefully study the effect of increasing Br concentration on the CVD reactions of ferrocene.

In particular through scanning electron microscopy (SEM), energy dispersive X-rays (EDX), X-ray diffraction (XRD), transmission electron microscopy (TEM) and high resolution transmission electron microscopy (HRTEM) we demonstrate that thin walled CNTs filled with micrometre long Fe₃C single crystals can be synthesized by mixing 30 mg of ferrocene with very small quantities of (6-Bromohexyl)ferrocene (3.2 mg). Furthermore by fixing the quantity of ferrocene to that of 30 mg and varying the quantity of

⁺ These authors contributed equally to this work.

^a College of Physical Science and Technology, Sichuan University, 610064, Chengdu, China.

Email: f.boi@scu.edu.cn (*first corresponding author)

Email: gxiang@scu.edu.cn (** second corresponding author)

^b Analytical & Testing Center, Sichuan University, Chengdu, 610064, China

Electronic Supplementary Information (ESI) available

DOI: 10.1039/x0xx00000x

(6-Bromohexyl)ferrocene from 3.2 mg to 6.4 mg and to higher quantities up to 25.6 mg we show that a transition from thin walled CNTs with micrometre-length filling rates to tip-filled CNTs and to empty thin CNTs can be clearly found. We attribute this sharp transition to an etching interaction imposed by the formation of Br radicals in the pyrolyzed vapour and to the possible formation of metal-bromide species. EDX analyses indeed show the presence Br residues up to 2 weight % in the catalyst particles. Instead (see Fig.1 Supp Info) the pyrolysis of the only (6-Bromohexyl)ferrocene did not yield the growth of CNTs. We attribute this result to the high concentration of Br created in the pyrolyzed vapour by the extremely low Ar flow rates of 11 ml/min used in our CVD system. The CNTs-yield of the produced samples is measured through thermo-gravimetric analyses.

The morphology of the CNTs obtained by CVD of mixtures of 30 mg of ferrocene and 3.2 mg of (6-Bromohexyl)ferrocene (sample 1) was revealed by SEM micrographs taken from the CNTs-growth-area peeled-off from the surface of the Si/SiO₂ substrate extracted from the CVD reactor. A typical SEM micrograph is shown in Fig.1. As shown in Fig.1A the CNTs are found to grow from unusual films of Fe-based catalyst particles. These films are very different with respect to those generally obtained as product of the pyrolysis of the only ferrocene⁹⁻¹¹ (aligned films of CNTs). The film was peeled off from the substrate with a carbon film-tape for the SEM analyses. In order to observe the grown CNTs the attention was focused in the fractured regions of the catalyst-film. This can be observed with an high detail in Fig.1B where many CNTs connected to the catalyst-film are found. In particular the filling rate of the CNTs structures was revealed by backscattered electron micrographs. This technique can allow to observe the differences in atomic contrast between the Fe-based crystals inside the CNT-core and the CNT. The encapsulated crystals can be observed in the bright areas of Fig.1C and 1D. The red star indicates a typical example of encapsulated Fe-based crystal. In particular, as shown in Fig.1C-D the diameter of the encapsulated crystals is found to be in the range of 3-10 nm and typically increases at the capping point (region of CNTs closure) of each CNT and reaches a diameter of approximately 100-200 nm.

In order to investigate the morphological variation of the CNTs with the quantity of (6-Bromohexyl)ferrocene, the use of larger (6-Bromohexyl)ferrocene quantities corresponding to 6.4 mg, 12.8 mg and 25.6 mg respectively was considered; while the quantity of ferrocene was kept constant to 30 mg. The morphological properties of the CNTs obtained from CVD of 30 mg of ferrocene and 6.4 mg of (6-Bromohexyl)ferrocene mixtures (sample 2) was revealed by the SEM micrograph of the films grown on the Si/SiO₂ substrates and peeled-off through the same method used in the case of the first CNTs sample (shown in Fig.1). This can be observed in the SEM micrographs of Fig.2. As shown in Fig.2A-C, the CNTs obtained in this case have a characteristic tip-filled morphology, still characterized by a very small diameter but also by a strongly decreased filling rate. In the majority of cases each CNT is found with only one encapsulated crystal in the capping region (see Fig.2B), while the other parts of the CNTs core appear to be

completely empty. This can be observed in the backscattered electrons micrograph of Fig.2C where the bright areas represent the

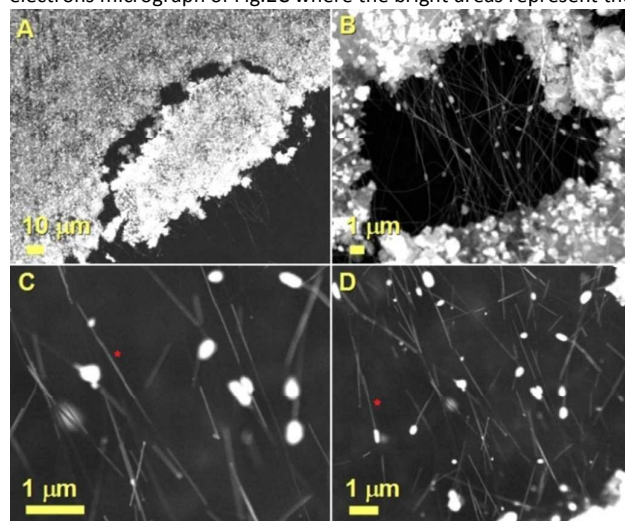


Fig. 1: Scanning electron micrographs of the sample 1 produced by CVD of 30 mg of ferrocene and 3.2 mg of (6-Bromohexyl)ferrocene showing: in A the morphology of the film of catalyst particles grown on the surface of the Si/SiO₂ substrates; in B many CNTs connected to the catalyst particles of the film and C-D the backscattered electron micrographs of the CNTs, which show the micrometre-length filling rate of each CNT.

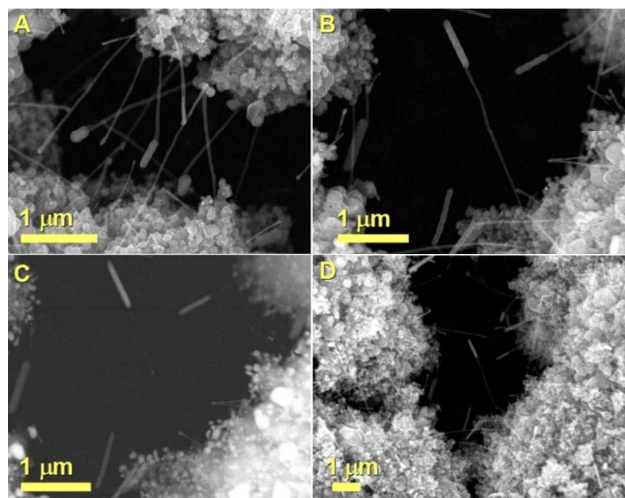


Fig. 2: Scanning electron micrographs of the sample 2 produced by CVD of 30 mg of ferrocene and 6.4 mg of (6-Bromohexyl)ferrocene showing in A the morphology of thin CNTs tip-filled with micrometre size Fe-based particles departing from the film of catalyst-particles grown on the surface of the Si/SiO₂ substrates. In B an high detail of typical CNTs obtained in this conditions is shown. In C the backscattered electron image shows more clearly (bright areas) the capping-position of the filling in the CNTs shown in B. In D a top view of the analyzed area is shown.

encapsulated crystals. A top view of the produced CNT can be also observed in Fig.2D. In order to investigate further the dependence of the CNTs filling rate on the quantity of (6-Bromohexyl)ferrocene mixed with ferrocene, further SEM investigations were then performed on the samples produced with 12.8 mg (sample 3) and 25.6 mg (sample 4) of (6-Bromohexyl)ferrocene (and 30 mg of

ferrocene). The morphology of the CNTs comprised in sample 3 is shown in Figs.3A-D. Also in this case the CNTs are found connected to films of catalyst particles peeled off from the Si/SiO₂ substrate with the same methods described above. A typical example of the film of catalyst particles peeled off from the substrate and of the CNTs produced in these conditions is shown in Fig.3A. The produced CNTs are also shown with a higher detail in Fig.3B. The CNTs diameter (30-50 nm) appear slightly larger with respect to that of the CNTs shown in Fig.1 and Fig.2. Furthermore, by comparing the direct SEM micrographs (see Fig.3C) with the backscattered electron analyses (see Fig.3D), a sharp morphological change of CNTs, with a complete disappearance of the encapsulated particles is surprisingly found. Similar results are also observed in the case of sample 4. Indeed also in this case as shown in the direct SEM micrograph of Fig.4A and the backscattered electron micrograph of Fig.4B, a complete disappearance of the CNTs-filling and a CNTs diameter of 30-50 nm are found (see Fig.4C). A top view of many CNTs connected to the film of catalyst particles is shown in Fig.4D. The use of EDX analyses was then considered: 1) to investigate the possible presence of Br residues in the CNTs or in the Fe₃C catalyst due to etching interaction with Br radicals and to understand more the sharp transition from filled CNTs to empty CNTs 2) to investigate the possible dependence of these residues on the chemical reactions involved in the CVD process and on the quantity of (6-Bromohexyl)ferrocene used in each reaction. The EDX analyses together with the analyzed area of the CNTs previously shown in Fig.1 can be observed in Fig.2Supp-info. Together with C, Fe and O, also Br is found in the list of element present in the sample. This result is different with respect to the previous reports on Cl-methods where no Cl was found in the CNTs and in the encapsulated particles²⁴. In particular the weight % of Br in this case was 0.36%.

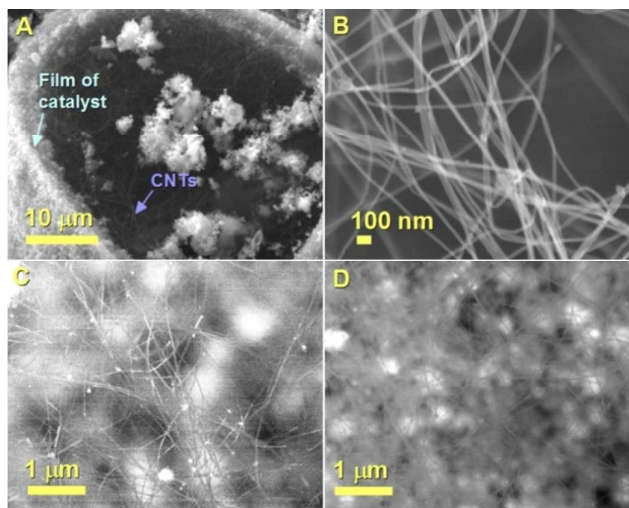


Fig.3: Scanning electron micrographs of the sample 3 produced by CVD of 30 mg of ferrocene and 12.8 mg of (6-Bromohexyl)ferrocene showing in A the morphology of a flake of the film of catalyst-particles grown on the surface of the Si/SiO₂ substrates and peeled off for the analyses. In B an high detail of typical CNTs obtained in this conditions is shown. In C and D a comparison between direct imaging and backscattered electrons imaging shows that in these conditions no particles are observed inside the CNTs.

These observations clearly suggest that a residue of Br is present either in the catalyst particles and/or in the CNTs. Further investigations were then performed to understand the variation of the Br weight % in the case of the CNTs shown in Figs.2-4 (sample 2-4). As shown in Fig.3 supp-info, an increase of the Br weight % to 0.54 (Fig.3 supp-info A) in the case of the CNTs previously observed in Fig. 2 (sample 2) and 2.36 (Fig.3 supp-info B) in the case of the CNTs previously shown in Fig.3 (sample 3) is found. This trend is also confirmed in the case of the sample 4, where a variable quantity of Br from 2 weight % to 1.2 weight % is found in different areas of the sample (Fig.3 supp-info C). Also, EDX analyses performed on isolated CNTs (Fig.3 supp-info D) show that no Br is present inside the CNTs. These analyses suggest that in our CVD conditions (see supp-info), Br radicals can etch the metal-catalysts, limiting the saturation rate and therefore the filling ratio of the CNTs. However due to the low spatial resolution of SEM the presence of Br in the CNTs can not be excluded. Also the formation of iron-bromide species is possible.

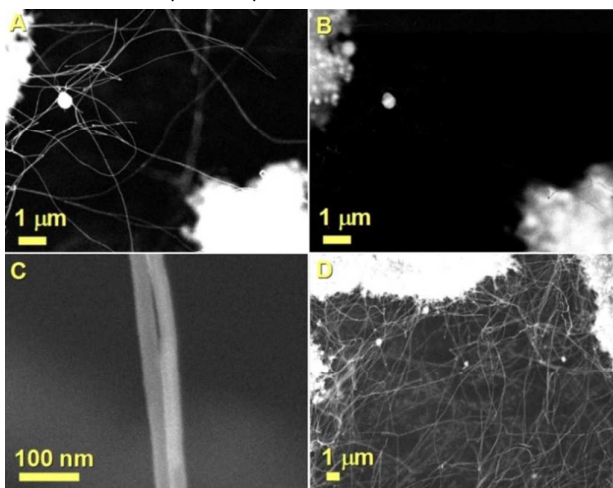


Fig.4: Scanning electron micrographs of the sample 4 produced by CVD of 30 mg of ferrocene and 25.6 mg of (6-Bromohexyl)ferrocene showing in A the morphology of typical CNTs obtained in these conditions and in B the backscattered electrons imaging which clearly shows that also in this conditions empty CNTs are obtained as dominant product. The typical diameter of the CNTs is shown with high detail in the micrograph of C where a typical diameter of 30 nm is measured. In D a top view of many CNTs connected to the film of catalyst particles is shown.

Other EDX performed in the catalysts-particles also confirm the presence of residues of Br up to 1 weight% (Fig.4 supp-info). In order to confirm these interpretations, and further investigate the structural-composition of sample 1 and sample 4, the use of XRD analyses was considered (in this case for each sample the CNTs and catalyst films were gently removed from the Si/SiO₂ with a spatula). A typical XRD diffractogram obtained from the analyses performed on the sample 1 is shown in Fig.5A. In addition to the 002 graphitic reflection (which can be referred to the CNTs and partially to spherical carbon layers surrounding the particles in the catalyst-film) labelled with red colour in Fig.5A, the presence of orthorhombic Fe₃C with space group Pnma was revealed by the

presence of the 210, 002, 201, 211, 102, 220, 031, 112, 131, 221 and 122 reflections (black labels). The Fe_3C reflections were identified by using the database card number 1008725. Further XRD analyses were then performed in the sample 4. The obtained XRD pattern can be observed in Fig.5B. Also in this case the presence of CNTs was revealed by the 002 graphitic reflection, however the intensity of the observed peak appear to be much lower with respect to that observed in the case of Fig.5A, suggesting that the number of CNTs walls decrease with the increase of the quantity of 6-Bromohexyl)ferrocene. Similarly also the intensity of the reflections associated to the Fe_3C orthorhombic structure (see Fig.5B) show a sudden decrease.

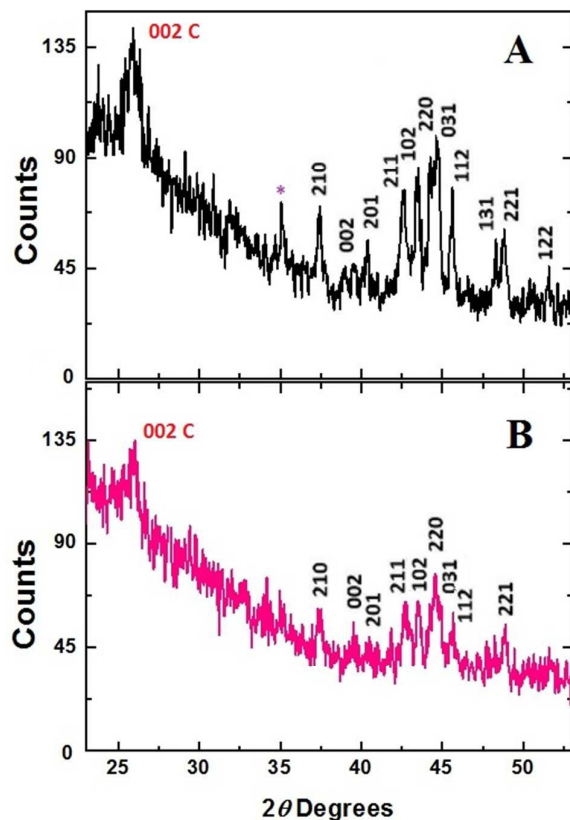


Fig.5: XRD analyses showing in A the diffractogram of the sample 1 and in B the diffractogram of the sample 4. The magenta star in A refers to the 200 reflection of Fe_3C which surprisingly has a remarkable intensity, despite the low-intensity predicted by the database-card 1008725 ICSD.

This unusual decrease in the intensities of the 002 graphitic reflection and Fe_3C atomic structure reflections can be related to the formation of Br radicals which would 1) etch the Fe_3C catalyst, as confirmed by EDX in the Fe_3C particles, or 2) etch the CNTs, decreasing the number of CNTs-walls, 3) form metalbromide species which could be favoured in presence of large quantities of Br in the pyrolyzed vapour and that could explain the decreased quantity of Fe_3C in Fig.5B. In order to investigate further the cross-sectional morphology and the structural composition of the produced CNTs and encapsulated crystals, the sample 1, sample 2

and sample 4 were analyzed by TEM and HRTEM. A typical example of many thin CNTs with a micrometre-length filling rate (sample 1) is shown in Fig.6A. The diameter of the encapsulated crystals was investigated through HRTEM. As shown in Fig.6B-D the diameter of the encapsulated crystals resulted to be in the range of 3-10 nm (measured through analyses of 50 crystals in multiple TEM sessions), while the number of CNTs walls was found to be approximately 20 or 30. The HRTEM micrograph of Fig.6C and Fig.6D allowed also to study the structure of the encapsulated crystals. In particular the atomic lattice spacings of 0.21 nm measured in the case of Fig.6C correspond to the 211 reflections of Fe_3C with space group Pnma. Similarly, the lattice spacings of 0.44 nm observed in Fig.6D correspond to the 001 reflection of Fe_3C with space group Pnma²⁶.

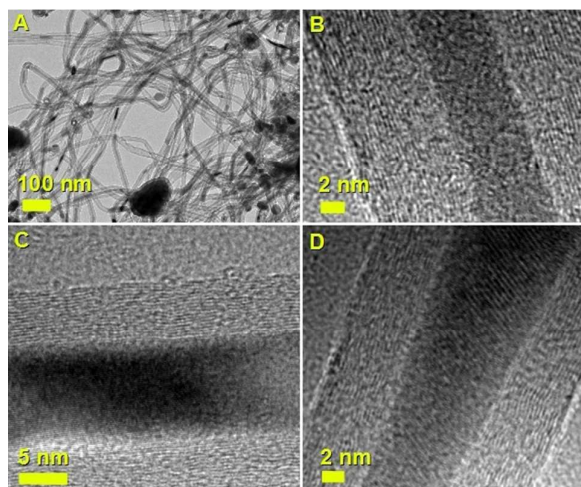


Fig.6: Transmission electron micrographs of the sample 1 showing in A the cross-sectional morphology of thin walled CNTs filled with micrometre length Fe-based particles. The size of the encapsulated particles ranges from 3-10 nm (see B-D). The atomic structure arrangement of these particles is analyzed in C and D with HRTEM imaging of typical CNTs obtained in these conditions. The atomic lattice spacings of the encapsulated crystals shown in C and D refer to the 211(C) and 001 (D) reflections of Fe_3C with space group Pnma²⁶.

Further TEM analyses were then performed on the tip-filled CNTs comprised in sample 2. A typical TEM micrograph showing a single tip-filled CNT can be observed in Fig.7. Similarly to what shown by the SEM micrographs, only the final part of these CNTs is filled with single Fe_3C particles, while the rest of the thin-walled CNTs core is found to be empty. Due to the localized position of these ferromagnetic crystals in the tip of the CNTs, these nanostructures could be considered suitable candidates for production of buckypapers with magnetic properties localized only on one end of the CNTs^{3-5,21}. The TEM analyses were then performed on the CNTs comprised in the sample 4. In agreement to what previously observed in the case of the SEM analyses of Fig.4, in this case metal-free thin walled CNTs were obtained as dominant product in the reactor. Typical TEM micrographs of these nanostructures are shown in Fig.8 and indicated in Fig.8A-C with the blue arrows. In Fig.8D a high detail of a typical metal-free CNT is shown. The catalyst particles detached from the catalyst-film on the Si/SiO_2

substrate surface are indicated with red arrows. In the majority of cases these particles are found surrounded with graphitic layers in an onion like structure which could be obtained during the cooling process. The low-intensity Fe_3C reflections observed in Fig.5B can be therefore associated to the catalyst-film. While the 002 graphitic peak observed in Fig.5 (as mentioned above) can be partially associated to the carbon layers which surrounds the Fe_3C -particles in the catalyst film.

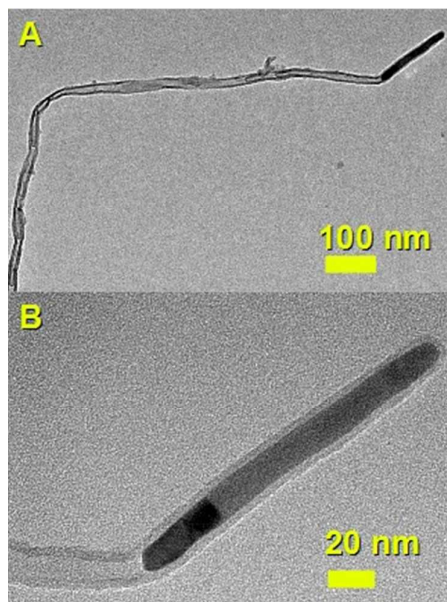


Fig.7: Transmission electron micrographs of the sample 2 showing in A the cross-sectional morphology of a thin walled CNT filled only in the tip region with a thin elongated Fe_3C particle. A high detail of the particle is shown in B. These observations suggest a tip-growth mechanism⁶.

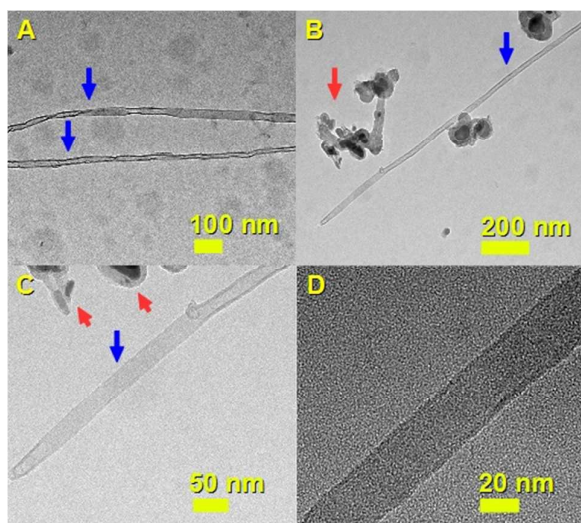


Fig.8: Transmission electron micrographs of the sample 4 showing in A the cross-sectional morphology of two metal-free thin walled (7-10 walls) CNTs. Another example of metal free CNT is shown in B and C. In D an high detail of a metal free CNT is shown. The blue arrows indicate the metal-free CNTs, the red arrows indicate examples of the morphology of the catalyst detached from the film during the TEM sample preparation after dispersion in ethanol.

Considering that TEM can offer also a higher spatial resolution with respect to SEM, the use of scanning TEM (STEM) mode was then considered to further investigate the presence of Br inside the CNTs or in the encapsulated crystals. In particular STEM analyses were performed on encapsulated micrometre long single crystals of Fe_3C (see Fig.5 supp-info for electron diffraction pattern) prepared from sample 1 and on empty CNTs prepared from sample 4 (see Fig.9). The EDX analyses (see Fig.9 BCD) of the areas 1-3 of the analyzed CNTs revealed the presence of Br in both the filled and empty regions of the CNT prepared from sample 1. Furthermore, as shown in Fig.9E-F, similar results were obtained also in the case of the CNTs prepared from sample 4. However in this case the presence of small quantities of Si was found. This could be associated to the high reactivity of halides with the Si present in the substrate.

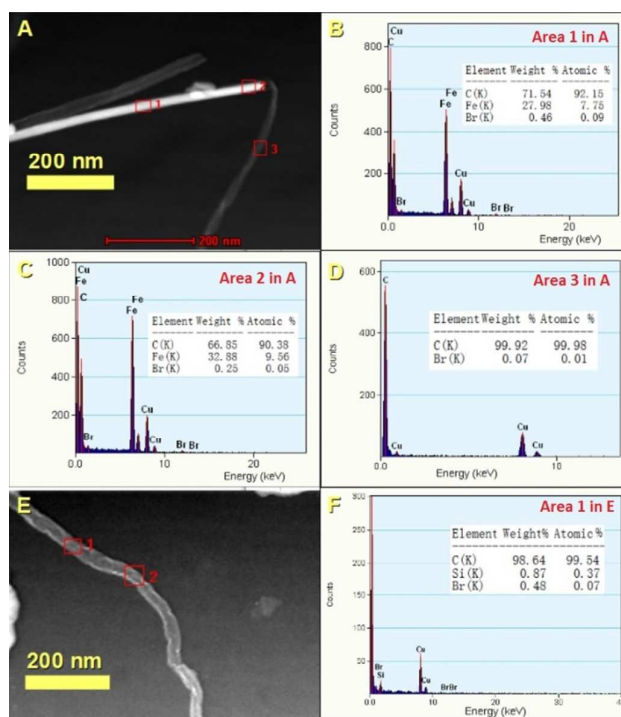


Fig.9: In A, scanning transmission electron micrograph three areas of a typical filled CNT chosen for EDX analyses. The EDX analyses are shown in B-D. The micrograph in E shows two areas of a typical empty CNT chosen for EDX analyses. The EDX analysis showing the composition of the empty CNT in the area 1 is shown in F as typical example.

Being interested in evaluating the yield of CNTs comprised in sample 1 (comprising CNTs with micrometre-long filling) and sample 4 (comprising empty CNTs), the use of TGA analyses was considered.

The TGA measurements (in air) are shown in Fig.10. The weight-loss observed at about 500-650 °C is due to the CNTs decomposition, while the weight residues observed after this process correspond to the film-particles. The weight losses due to CNTs decomposition correspond to 55% for the sample 1 (black curve) and to 61.6 % for sample 4 (red curve).

In particular the weight residue observed for the sample 1 (black curve) corresponds to 45.0 %, while the weight residue observed for sample 4 (red curve) corresponds to 38.4 %. These observations suggest that the quantity of metal-carbide comprised in the samples decreases with the increase of the (6-Bromohexyl)ferrocene quantity.

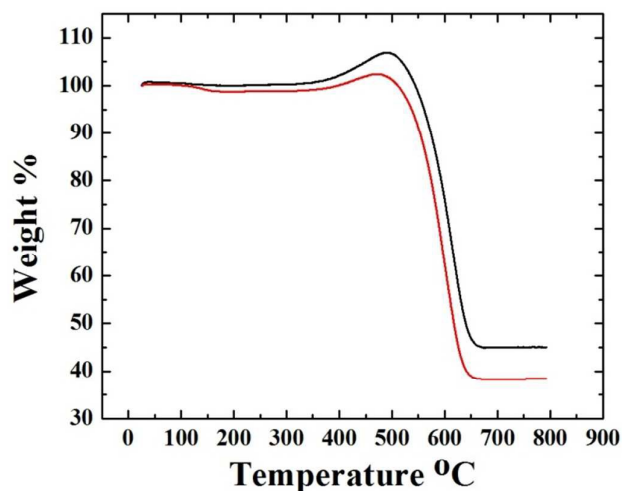


Fig.10: Thermogravimetric analyses of the sample 1 (black curve) and sample 4 (red curve). The weight loss observed at about 500-650 °C is due to the CNTs decomposition. The residues observed after this process correspond to the film-particles.

In conclusion we reported an advanced synthesis approach based on the CVD of ferrocene with a not previously used precursor: (6-Bromohexyl)ferrocene with the purpose of studying the role of Br in the CVD of ferrocene. Thin walled CNTs filled with micrometre long Fe_3C single crystals were obtained as result of CVD of 30 mg of ferrocene with 3.2 mg of (6-Bromohexyl)ferrocene. Differently a tip-filled morphology is observed with the increase of the (6-Bromohexyl)ferrocene to 6.4 mg. Also, by further increasing the quantity of (6-Bromohexyl)ferrocene to 25.6 mg a sharp transition from Fe_3C -filled CNTs to metal-free CNTs was found. This is confirmed by SEM, XRD and TEM analyses. Furthermore through EDX analyses of each sample we have shown that this transition can be attributed to the formation of Br radicals which can etch the Fe_3C -catalyst and also to the possible formation of metal-bromide which could then be removed from the reactor in the form of gas-phase. We suggest that the produced CNTs are suitable candidates for fabrication of nanotube films and buckypapers through purification and filtration methods for applications as magnetic sensors, electrodes and super capacitors^{3-5,21} and other buckypapers where the magnetic properties are instead localized in the tip of the CNTs.

Acknowledgements:

We acknowledge professor Gong Min for his continuous support to this research project and we acknowledge the support from the start-up funding of Sichuan University.

References

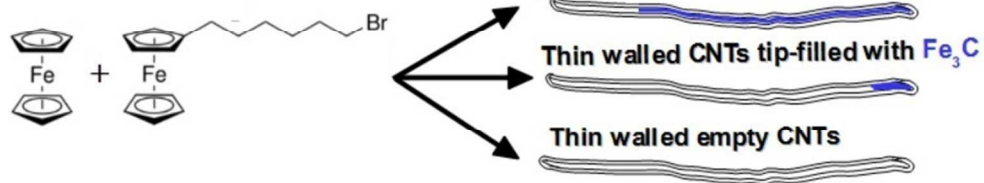
- 1M. S. Dresselhaus, G. Dresselhaus, P. Avouris, Carbon Nanotubes: Synthesis, Structure, Properties, and Applications, Springer, Berlin 2001.
- 2 J. Kong, E. Yenilmez, T. W. Tomblor, W. Kim, H. J. Dai, R. B. Laughlin, L. Liu, C. S. Jayanthi, S. Y. Wu. Phys. Rev. Lett. 2001, **87**, 106 801.
- 3 M. T. Byrne, Y.K. Gunko. Advanced Materials. 2010, **22**, 1672–1688.
- 4 W. Ding, S. Pengcheng, L. Changhong, W. Wei, F. Shoushan. Nanotechnology, 2008, **7**, 075609.
- 5 P.D. Bradford, X. Wang, H. Zhao, J.P. Maria, Q. Jia, Y.T. Zhu. Composites Science and Technology 2010, **70**, 1980–1985.
- 6 U. Weissker, S. Hampel, A. Leonhardt, B. Buchner. Materials 2010, **3**, 4387.
- 7 F. C. Dillon, A. Bajpai, A. Koos, S. Downes, Z. Aslam and N. Grobert. Carbon, 2012, **50**, 3674.
- 8 A. Morelos-Gomez, F. Lopez-Urias, E. Munoz-Sandoval, C. L. Dennis, R. D. Shull, H. Terrones and M. Terrones. Journal of Material Chemistry, 2010, **20**, 5906.
- 9 S. Hampel, A. Leonhardt, D. Selbmann, K Biedermann, D. Elefant, Ch. Muller, T. Gemming and B. Buchner. Carbon 2006, **44**, 2316.
- 10 A. Leonhardt, M. Ritschel, R. Kozhuharova, A. Gra_a, T. Muhl, R. Huhle, I. Monch, D. Elefant and C.M. Schneider Diamond and Related Materials, 2003, **12**, 790.
- 11 A. Leonhardt, M. Ritschel, M.; Elefant, D. N. Mattern, K. Biedermann, S. Hampel, Ch. Muller, T. Gemming, B. Buchner. Journal of Applied Physics, 2005, **98**, 074315.
- 12 J. A. Rodríguez-Manzo, M. Terrones, H. Terrones, H.W. Kroto, L. Sun, F. Banhart. Nature Nanotechnology, 2007, **2**, 307.
- 13 U. Weissker, M. Lo_er, F. Wolny, M. U.Lutz, N. Scheerbaum, R. Klingeler, T. Gemming, T. Muhl, A. Leonhardt and B. Buchner J. Appl. Phys., 106, 054909 (2009).
- 14 M. U. Lutz, U. Weissker, F. Wolny, C. Muller, M. Lo_er, T. Muhl, A. Leonhardt, B. Buchner and R. Klingeler. Journal of Physics: Conference Series, 200, 072062 (2010).
- 15 N. Grobert, M. Mayne, M. Terrones, J. Sloan, R. E. Dunin-Borkowski, R. Kamalakaran, T. Seeger, H. Terrones, M. Ruhle, D. R. M. Walton, H. W. Kroto and J. L. Hutchison. Chem. Commun., 2001, 471–2
- 16 A.L. Elias, J. A. Rodriguez-Manzo, M. R. McCartney, D. Golberg, A. Zamudio, S. E. Baltazar, F. Lopez-Urias, E. Munoz-Sandoval, L. Gu, C. C. Tang, D. J. Smith.; Y. Bando, H. Terrones, M. Terrones. Nano Lett., 2005, **5**, 467.
- 17 F. S. Boi, G. Mountjoy, R. M. Wilson, Z. Luklinska, L. J. Sawiak, M. Baxendale. Carbon, 2013, **64**, 351.
- 18 F. S. Boi, R. M. Wilson, G. Mountjoy, I. Muhammad, M. Baxendale. Faraday Discussions, 2014, **173**, 67.
- 19 F. S. Boi, G. Mountjoy, M. Baxendale. Carbon, 2013, **64**, 516.

Journal Name

ARTICLE

- 20 R. Lv, F. Kang, J. Gu, X. Gui, J. Wei, K. Wang and D. Wu. Applied Physics Letters, 2008, **93**, 223105.
- 21 R. Lv, S. Tsuge, X. Gui, K. Takai, F. Kang, T. Enoki, J. Wei, J. Gu, K. Wang, D. Wu Carbon, 2009, **47**, 1141.
- 22 R. Lv, F. Kang, W. Wang, J. Wei, J. Gu, K. Wang, D. Wu. Carbon 2007, **45**, 1433.
- 23 X. Gui, K. Wang, W. Wang, J. Wei, X. Zhang, R. Lv, Y. Jia, Q. Shu, F. Kang, D. Wu. Materials Chemistry and Physics, 2009, **113**, 634–637
- 24 R. Lv, A. Cao, F. Kang, W. Wang, J. Wei, J. Gu, K. Wang, and D. Wu. J. Phys. Chem. C 2007, **111**, 11475.
- 25 Z Wang, X Liu, M Lv, J Meng. Carbon, 2010, **48**, 3182.
- 26 F. S. Boi, G. Mountjoy, Z. Luklinska, L. Spillane, L. S. Karlsson, R. M. Wilson, A. Corrias and M. Baxendale. Microscopy and Microanalysis, 2013, **19**, 1298.

CVD in Ar at 990 °C



196x57mm (120 x 120 DPI)